

Static and dynamic properties of the XXZ chain with long-range interactions

L. L. Gonçalves^{a*}, L. P. S. Coutinho^a, J. P. de Lima^b

^(a)Departamento de Física, Universidade Federal do Ceará,
Campus do Pici, caixa postal 6030, 60451-970 Fortaleza, Ceará, Brazil

^(b)Departamento de Física, Universidade Federal do Piauí,
Campus Ministro Petrônio Portela, 64049-550, Teresina, Piauí, Brazil

Abstract

The one-dimensional XXZ model ($s=1/2$) in a transverse field, with uniform long-range interactions among the transverse components of the spins, is studied. The model is exactly solved by introducing the Jordan-Wigner transformation and the integral Gaussian transformation. The complete critical behaviour and the critical surface for the quantum and classical transitions, in the space generated by the transverse field and the interaction parameters, are presented. The crossover lines for the various classical/quantum regimes are also determined exactly. It is shown that, besides the tricritical point associated with the classical transition, there are also two quantum critical points: a bicritical point where the classical second-order critical line meets the quantum critical line, and a first-order transition point at zero field. It is also shown that the phase diagram for the first-order classical/quantum transitions presents the same structure as for the second-order classical/quantum transitions. The critical classical and quantum exponents are determined, and the internal energy, the specific heat and the isothermal susceptibility, χ_T^{zz} , are presented for the different critical regimes. The two-spin static and dynamic correlation functions, $\langle S_j^z S_l^z \rangle$, are also presented, and the dynamic susceptibility, $\chi_q^{zz}(\omega)$, is obtained in closed form. Explicit results are presented at $T = 0$, and it is shown that the isothermal susceptibility, χ_T^{zz} , is different from the static one, $\chi_q^{zz}(0)$. Finally, it is shown that, at $T = 0$, the internal energy close to the first-order quantum transition satisfies the scaling form recently proposed by Continentino and Ferreira.

Key words: one-dimensional XXZ model; long-range interaction; classical-quantum crossover; dynamic properties; quantum phase transition.

PACS: 05.70.Ce; 05.70.Fh; 05.70.Jk; 75.10.Jm

Preprint submitted to PHYSICA A.

*Email address lindberg@fisica.ufc.br (L. L. Gonçalves).

1 Introduction

Quantum transitions are induced by quantum fluctuations which occur in the limit of very low temperatures ($T \rightarrow 0$), where they dominate over thermal fluctuations responsible for inducing classical transitions [1]. The Mott transition, between extended and localized electronic states, is perhaps the best known and studied example of quantum transitions (metal-insulator transition) [2].

The observation of anomalous behaviour in magnetic materials at very low temperatures has stimulated the study of the quantum transitions in these systems [3,4]. In particular, since the transitions occur at $T = 0$, the study of magnetic chains is particularly welcome in view of the possibility of obtaining exact solutions which allow a rigorous description. This has been the main motivation for considering in this work the XXZ chain, with a uniform long-range interaction, where quantum and classical transitions are allowed and an exact solution can be obtained. Although the model has already been considered by Suzuki [5], his study was restricted to the analysis of the classical second-order transition. As it will be shown, besides first-order classical transitions, the model also presents quantum transitions of first and second-order. This model is amenable to rigorous study of the classical/ quantum crossover. Since we are interested in the complete description of the critical behaviour (quantum and classical transitions of first and second-order), it will be considered again.

In section 2 we present the solution of the model and obtain the equation of state. The classical critical behaviour is obtained in section 3, and the quantum critical one in section 4. The dynamic correlations in the field direction are studied in section 5 and in section 6 we present the dynamic susceptibility. Finally, in section 7, we obtain the critical surface for the quantum and classical transitions, and the crossover lines separating the various critical regimes.

2 Basic results and the equation of state

We consider the one-dimensional XXZ model ($s = 1/2$, N sites) with uniform long-range interactions among the z components of the spins. The Hamiltonian is explicitly given by

$$H = -J \sum_{j=1}^N (S_j^x S_{j+1}^x + S_j^y S_{j+1}^y) - \frac{I}{N} \sum_{j,k=1}^N S_j^z S_k^z - h \sum_{j=1}^N S_j^z, \quad (1)$$

where N is the number of sites of the lattice and we have assumed periodic boundary conditions. By applying the Jordan-Wigner fermionization [6,7],

$$S_j^+ = \left[\exp \left(i\pi \sum_{l=1}^{j-1} c_l^\dagger c_l \right) \right] c_j^\dagger; \quad S_j^- = c_j \left[\exp \left(-i\pi \sum_{l=1}^{j-1} c_l^\dagger c_l \right) \right], \quad (2)$$

this Hamiltonian can be written in the form

$$\begin{aligned}
H = & -\frac{J}{2} \sum_{j=1}^N \left(c_j^\dagger c_{j+1} + c_{j+1}^\dagger c_j \right) - (h - I) \sum_{j=1}^N c_j^\dagger c_j - \\
& - \frac{I}{N} \sum_{j,l=1}^N c_j^\dagger c_j c_l^\dagger c_l + \frac{N}{2} \left(h - \frac{I}{2} \right).
\end{aligned} \tag{3}$$

The partition function is then given by

$$\begin{aligned}
Z_N = & \exp \left[-\frac{\beta N}{2} \left(h - \frac{I}{2} \right) \right] Tr \left\{ \exp \left[\frac{\beta J}{2} \sum_{j=1}^N \left(c_j^\dagger c_{j+1} + c_{j+1}^\dagger c_j \right) \right] \times \right. \\
& \times \exp \left[\beta (h - I) \sum_{j=1}^N c_j^\dagger c_j + \frac{\beta I}{N} \sum_{j,l=1}^N c_j^\dagger c_j c_l^\dagger c_l \right] \left. \right\},
\end{aligned} \tag{4}$$

where $\beta = 1/(k_B T)$ and T is the temperature. It should be noted that the term with long-range interactions commutes with the Hamiltonian. This decomposition allows the introduction, in the second exponential, of the Gaussian transformation [8]

$$\exp(a^2) = \frac{1}{\sqrt{2\pi}} \int_{-\infty}^{\infty} \exp \left(-\frac{x^2}{2} + \sqrt{2}ax \right) dx, \tag{5}$$

such that the partition function can be written in the integral representation

$$\begin{aligned}
Z_N = & \exp \left[-\frac{N}{2} \left(\bar{h} - \frac{1}{2} \right) \right] \sqrt{\frac{N}{2\pi}} \int_{-\infty}^{\infty} \exp \left(-\frac{N\bar{x}^2}{2} \right) \times \\
& \times Tr \left\{ \exp \left[\frac{\bar{J}}{2} \sum_{j=1}^N \left(c_j^\dagger c_{j+1} + c_{j+1}^\dagger c_j \right) + \left(\bar{h} - I + \sqrt{2\bar{I}\bar{x}} \right) \sum_{j=1}^N c_j^\dagger c_j \right] \right\} d\bar{x},
\end{aligned} \tag{6}$$

where $\bar{x} \equiv x/\sqrt{N}$, $\bar{J} \equiv \beta J$, $\bar{h} \equiv \beta h$ and $\bar{I} \equiv \beta I$.

Introducing the canonical transformation

$$c_k^\dagger = \frac{1}{\sqrt{N}} \sum_{j=1}^N \exp(-ikj) c_j^\dagger, \tag{7}$$

with $k = 2\pi n/N$, $n = 1, 2, 3, \dots, N$, eq. (6) can finally be written in the form

$$Z_N = C(\beta) \int_{-\infty}^{\infty} \exp \left(-\frac{N^2}{2} \right) \zeta(\bar{x}) d\bar{x}, \tag{8}$$

where

$$C(\beta) \equiv \sqrt{\frac{N}{2\pi}} \exp \left[-\frac{N}{2} \left(\bar{h} - \frac{1}{2} \right) \right], \quad \zeta(\bar{x}) \equiv Tr \left\{ \exp \left[\sum_k \bar{\epsilon}_k(\bar{x}) c_k^\dagger c_k \right] \right\}, \tag{9}$$

and

$$\bar{\epsilon}_k(\bar{x}) = \beta \epsilon_k(\bar{x}) \equiv \beta \left(J \cos(k) + h - I + \sqrt{\frac{2I}{\beta}} \bar{x} \right). \quad (10)$$

In the thermodynamic limit, $N \rightarrow \infty$, the partition function can be calculated by Laplace's method [9],

$$Z_N = \frac{\exp \left[-\frac{N}{2} \left(\bar{h} - \frac{1}{2} \right) + N g(\bar{x}_0) \right]}{|g''(\bar{x}_0)|^{\frac{1}{2}}}, \quad \text{with} \quad g'(\bar{x}_0) = 0, g''(\bar{x}_0) < 0, \quad (11)$$

and where

$$g(\bar{x}) = -\frac{\bar{x}_0^2}{2} + \frac{1}{N} \sum_k \ln [1 + \exp(\bar{\epsilon}_k)]. \quad (12)$$

The Helmholtz free energy is given by

$$\mathfrak{F}_N = \frac{N}{2} \left(h - \frac{I}{2} \right) - N k_B T g(\bar{x}_0) + \frac{k_B T}{2} \ln |g''(\bar{x}_0)|, \quad (13)$$

where \bar{x}_0 is expressed in terms of the magnetization per site M^z ,

$$\begin{aligned} M^z &= \frac{1}{N} \sum_j \langle S_j^z \rangle = \frac{1}{N} \sum_k \langle c_k^\dagger c_k \rangle - \frac{1}{2} \\ &= \frac{1}{N} \sum_k \frac{1}{1 + \exp[-\bar{\epsilon}_k(\bar{x}_0)]} - \frac{1}{2}. \end{aligned} \quad (14)$$

Using eqs. (11) and (12), in the thermodynamic limit, we have

$$M^z + \frac{1}{2} = \frac{\bar{x}_0}{\sqrt{2I}}. \quad (15)$$

From this result it follows that the functional of the Helmholtz free energy per site is finally given by

$$\mathfrak{f} = \frac{h}{2} - \frac{k_B T}{\pi} \int_0^\pi \ln \{1 + \exp[\bar{\epsilon}_k(M^z)]\} dk + I M^z (M^z + 1), \quad (16)$$

where

$$\bar{\epsilon}_k(M^z) = -\bar{J} \cos(k) - \bar{h} - 2\bar{I} M^z. \quad (17)$$

The equation of state is obtained from eq. (16) by imposing the conditions

$$\frac{\partial \mathfrak{f}}{\partial M^z} = 0, \quad \text{with} \quad \frac{\partial^2 \mathfrak{f}}{\partial M^{z2}} > 0. \quad (18)$$

We then have

$$M^z = \frac{1}{2\pi} \int_0^\pi \tanh \left[\frac{\cos(k) + \Gamma + 2r M^z}{2\tilde{T}} \right] dk, \quad (19)$$

where $r \equiv I/J$, $\Gamma \equiv h/J$ and $\tilde{T} \equiv k_B T/J$.

3 The classical critical behaviour

For $I < 0$, the system is totally frustrated. Consequently, it does not present any classical critical behaviour. On the other hand, for $I > 0$, there is a classical critical behaviour; the system undergoes first and second-order transitions at a finite temperature.

The classical phase diagram is obtained from the equation of state, by considering $h = 0$. The second-order transitions are determined by taking in this equation the limit $M^z \rightarrow 0$, and the first-order classical transitions are obtained by solving the equations

$$M_t^z - \frac{1}{2\pi} \int_0^\pi \tanh \left[\frac{\cos(k) + 2rM_t^z}{2\tilde{T}_t} \right] dk = 0, \quad (20a)$$

$$\mathfrak{f}(M_t^z) = \mathfrak{f}(0), \quad (20b)$$

where M_t^z is the finite value of the magnetization at the transition. In passing we would like to note that eq.(19) reproduces the known results in the limits $J = 0$ [10] and $I = 0$ [11]. The first-order critical line meets the second-order line at the tricritical point, which can be obtained by imposing the condition that the second and fourth derivatives of the functional of the Helmholtz energy go to zero as $M^z \rightarrow 0$. This leads to the set of equations

$$\frac{r_{tr}}{2\pi\tilde{T}_{tr}} \int_0^\pi \text{sech}^2 \left[\frac{\cos(k)}{2\tilde{T}_{tr}} \right] dk - 1 = 0, \quad (21a)$$

$$\int_0^\pi \left\{ -2 \tanh^2 \left[\frac{\cos(k)}{2\tilde{T}_{tr}} \right] \text{sech}^2 \left[\frac{\cos(k)}{2\tilde{T}_{tr}} \right] + \text{sech}^4 \left[\frac{\cos(k)}{2\tilde{T}_{tr}} \right] \right\} dk = 0, \quad (21b)$$

from which we have $\tilde{T}_{tr} = 0, 37716\dots$ and $r_{tr} = 1, 39815\dots$. There is a critical value r_c , which is a lower bound for the first-order line, below which the system does not present classical behaviour; it corresponds to a first-order quantum transition. This point is determined by considering $M_t^z = 1/2$ and the limit $\tilde{T} \rightarrow 0$, in eqs.(20a) and (20b), which gives $r_c = 4/\pi$.

In a finite field, the critical line associated with the second-order transitions is obtained by requiring that the minimum of the functional of the Helmholtz free energy is triply degenerate. From eq.(16), this leads to the set of equations

$$\frac{1}{2\pi} \int_0^\pi \tanh \left[\frac{\bar{\epsilon}_k(M_{cr}^z)}{2} \right] dk - M_{cr}^z = 0, \quad (22a)$$

$$\frac{r}{2\pi\tilde{T}} \int_0^\pi \text{sech}^2 \left[\frac{\bar{\epsilon}_k(M_{cr}^z)}{2} \right] dk - 1 = 0, \quad (22b)$$

$$\frac{r^2}{\tilde{T}^2} \int_0^\pi \tanh \left[\frac{\bar{\epsilon}_k(M_{cr}^z)}{2} \right] \text{sech}^2 \left[\frac{\bar{\epsilon}_k(M_{cr}^z)}{2} \right] dk = 0, \quad (22c)$$

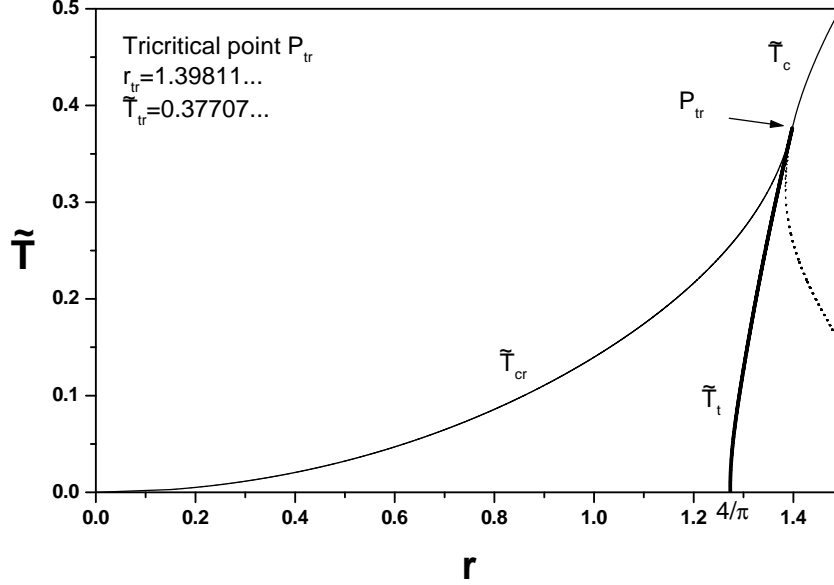


Figure 1: Phase diagram for the classical transitions as a function of the strength of the long-range interaction r ($r = I/J$). \tilde{T}_t ($\tilde{T}_t = k_B T_t/J$) identifies the first-order boundary, \tilde{T}_c ($\tilde{T}_c = k_B T_c/J$) the second-order critical line, P_{tr} the tricritical point and the \tilde{T}_{cr} ($\tilde{T}_{cr} = k_B T_{cr}/J$) the critical line at nonzero field.

where r_{cr} is restricted to the interval $0 < r_{cr} < r_{tr}$.

The classical phase diagram shown in Fig.1 can be constructed by solving eqs.(20-22). As it can be seen, below the tricritical point there is a curve of pseudo second-order transitions which correspond to metastable solutions. This classical phase diagram is very similar to analogous phase diagram of an Ising model with short and long-range interactions [12], as it will be shown below, is characterized by the same (mean-field) exponents.

The critical exponent β associated with the magnetization can be determined from eqs. (19), (21) and (22). It is found to be equal to $1/2$ for the second-order transitions and along the classical critical line, at nonzero field, and equal to $1/4$ at the tricritical point.

The classical transitions can also be characterized by the non-analytical behaviour of other thermodynamic functions. In particular, the internal energy and specific heat present non-analytical behaviour which are related to the order of the transition [10]. In order to analyze these behaviours let us consider the internal energy $U \equiv \langle H \rangle$. Using eqs. (3) and

(7), we can write

$$U = \sum_k \varepsilon_k \langle n_k \rangle - \frac{I}{N} \sum_{kk'} \langle n_k n_{k'} \rangle + \frac{N}{2} \left(h - \frac{I}{2} \right), \quad (23)$$

where ε_k and $\langle n_k \rangle$ are given by

$$\varepsilon_k = -J \cos(k) - h + I, \quad (24a)$$

$$\langle n_k \rangle = \frac{1}{1 + \exp[\bar{\varepsilon}_k(M^z)]}. \quad (24b)$$

By using Wick's theorem [13], the average $\langle n_k n_{k'} \rangle$ can be written in the form

$$\langle n_k n_{k'} \rangle = \langle n_k \rangle \langle n_{k'} \rangle + \langle c_k^\dagger c_{k'} \rangle \langle c_k c_{k'}^\dagger \rangle + \langle c_k^\dagger c_{k'}^\dagger \rangle \langle c_k c_{k'} \rangle. \quad (25)$$

From this result, and bearing in mind that $\langle c_k^\dagger c_{k'}^\dagger \rangle = \langle c_k c_{k'} \rangle = 0$, we can write the internal energy as

$$\begin{aligned} U &= \sum_k \varepsilon_k \langle n_k \rangle + \frac{N}{2} \left(h - \frac{I}{2} \right) - \\ &\quad - \frac{I}{N} \sum_{kk'} \langle n_k \rangle \langle n_{k'} \rangle - \frac{I}{N} \sum_k \langle n_k \rangle + \frac{I}{N} \sum_k \langle n_k \rangle^2. \end{aligned} \quad (26)$$

In the thermodynamic limit, we can write the internal energy per site u ($u = U/N$) in the explicit form

$$u = \frac{1}{\pi} \int_0^\pi \frac{\varepsilon_k}{1 + \exp[\bar{\varepsilon}_k(M^z)]} - IM^z (M^z + 1) + \frac{1}{2} (h - I), \quad (27)$$

which reproduces the known results for $J = 0$ [14] and $I = 0$ [15].

The specific heat, given by $c_h = (\partial u / \partial T)_h = -(\partial u / \partial \beta)_h / k_B T^2$, can be written as

$$\begin{aligned} \frac{c_h}{k_B} &= \frac{1}{\pi \tilde{T}^2} \left\{ \int_0^\pi \frac{(\cos(k) + \Gamma)^2 \exp(-\bar{\varepsilon}_k)}{[1 + \exp(-\bar{\varepsilon}_k)]^2} dk + \right. \\ &\quad + \left(4rM^z + \frac{2r}{\tilde{T}} \frac{\partial M^z}{\partial \beta} \Big|_h \right) \int_0^\pi \frac{(\cos(k) + \Gamma) \exp(-\bar{\varepsilon}_k)}{[1 + \exp(-\bar{\varepsilon}_k)]^2} dk + \\ &\quad \left. + 2rM^z \left(2rM^z + \frac{2r}{\tilde{T}} \frac{\partial M^z}{\partial \beta} \Big|_h \right) \int_0^\pi \frac{\exp(-\bar{\varepsilon}_k)}{[1 + \exp(-\bar{\varepsilon}_k)]^2} dk \right\}, \end{aligned} \quad (28)$$

where

$$\frac{\partial M^z}{\partial \beta} \Big|_h = \frac{\frac{1}{\pi} \int_0^\pi \frac{(\cos(k) + \Gamma + 2rM^z) \exp(-\bar{\varepsilon}_k)}{1 + \exp(-\bar{\varepsilon}_k)} dk}{1 - \frac{2r}{\pi \tilde{T}} \int_0^\pi \frac{\exp(-\bar{\varepsilon}_k)}{1 + \exp(-\bar{\varepsilon}_k)} dk}, \quad (29)$$

and, naturally, the values of M^z also satisfy the equation of state.

Typical results for the internal energy and the specific heat are shown in Fig. 2. As it can be seen in Fig. 2(a), where we have a classical first-order phase transition, the internal energy is discontinuous at the critical temperature (there is a latent heat associated with the transition) and the specific heat is singular but finite at this point. As shown in Fig. 2(b), where we have second-order transitions, the specific heat is also finite at the transition. However, it can be shown that it diverges at the tricritical point. The critical exponent α associated with the specific heat is equal to zero along the second-order transition line and $1/2$ at the tricritical point, which, as already pointed out, is the mean-field result.

The critical behaviour of the internal energy and specific heat along the critical line, is identical to the one at the tricritical point. Therefore, as expected, the exponent α is equal to $1/2$.

The classical critical behaviour can also be characterized by the isothermal susceptibility χ_T^{zz} . From the equation of state, eq.(19), we have

$$\chi_T^{zz} = \frac{\frac{1}{4\pi T} \int_0^\pi \text{sech}^2 \left(\frac{\cos(k) + \Gamma + 2rM^z}{2T} \right) dk}{1 - \frac{r}{2\pi T} \int_0^\pi \text{sech}^2 \left(\frac{\cos(k) + \Gamma + 2rM^z}{2T} \right) dk}. \quad (30)$$

The results for the susceptibility, shown in Fig. 3, are in agreement with typical mean-field behaviour at first and second-order classical transitions. For the first-order transition, shown in Fig. 3(a), the susceptibility is singular but finite at the transition temperature. On the other hand, along the second-order transition line as well as along the critical line, and at the tricritical point, it diverges, although with different critical exponents γ . These divergences, which are signatures of second-order transitions, are shown in Figs. 3(b), 3(c) and 3(d). We have calculated γ and have found that it is equal to 1 at the tricritical point and along the second-order transition line, whereas it is equal to $1/2$ along the nonzero field critical line. It should be remarked that the exponents α, β and γ satisfy the Rushbrooke scaling relation, $\alpha + 2\beta + \gamma = 2$ [10], and that the classical critical behaviour belongs to the same universality class of the Ising model with short and long-range interactions[12].

4 The quantum critical behaviour

The quantum phase diagram is determined by from the functional of the Helmholtz free energy, in the limit $T \rightarrow 0$. For $J > 0$ (or $J < 0$) eq. (16) can be written as [16]

$$f = \frac{h}{2} - \frac{1}{\pi} \int_0^\varphi [J \cos(k) + h + 2IM^z] dk + IM^z (M^z + 1), \quad (31)$$

where φ is given by

$$\varphi = \arccos[-(\Gamma + 2rM^z)]. \quad (32)$$

Also, we have the explicit form

$$f = \frac{h}{2} - \frac{1}{\pi} [\sin(\varphi) + (h + 2IM^z) \varphi] + IM^z (M^z + 1). \quad (33)$$

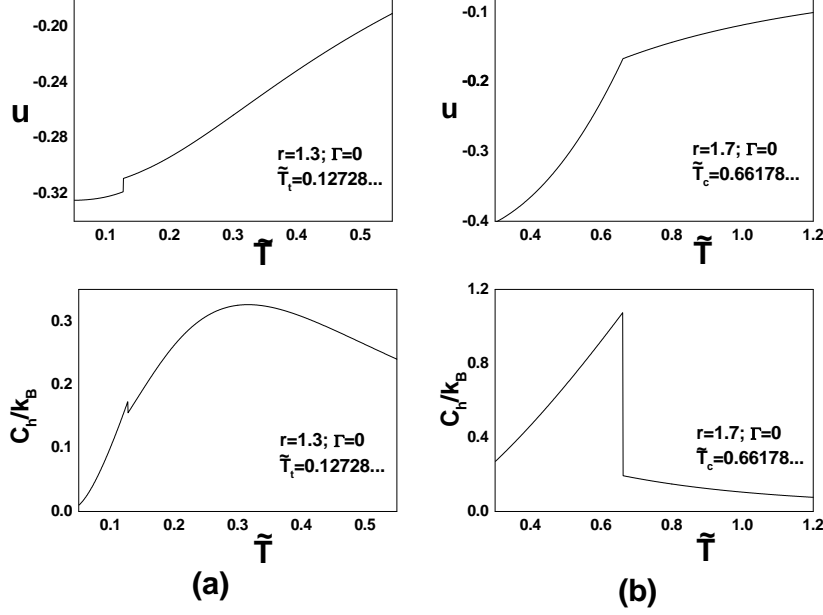


Figure 2: Internal energy (u) and specific heat c_h , at zero field, as a function of temperature. (a) For $r=1.3$ ($r = I/J$) where the system undergoes a classical first-order transition. (b) For $r=1.7$ where the system undergoes a classical second-order transition.

As in the classical region, the equation of state is obtained by imposing the conditions shown in eq.(18). Then we have

$$M^z = \frac{1}{\pi} \arccos [- (\Gamma + 2rM^z)] - \frac{1}{2}, \quad (34)$$

which corresponds to the equation of state, provided the condition of minimum of f is satisfied.

For $I > 0$ the system presents first-order transitions induced by the field, which are determined by the condition

$$f(M_t^z) = f\left(\frac{1}{2}\right). \quad (35)$$

Together with eq. (34) this leads to the system of equations

$$M_t^z + \frac{1}{2} - \frac{1}{\pi} \arccos [- (\Gamma_t + 2rM_t^z)] = 0, \quad (36a)$$

$$-\frac{1}{\pi} [\sin(\varphi_t) + (\Gamma_t + 2rM_t^z) \varphi_t] + rM_t^z (M_t^z + 1) + \Gamma_t + \frac{r}{4} = 0, \quad (36b)$$

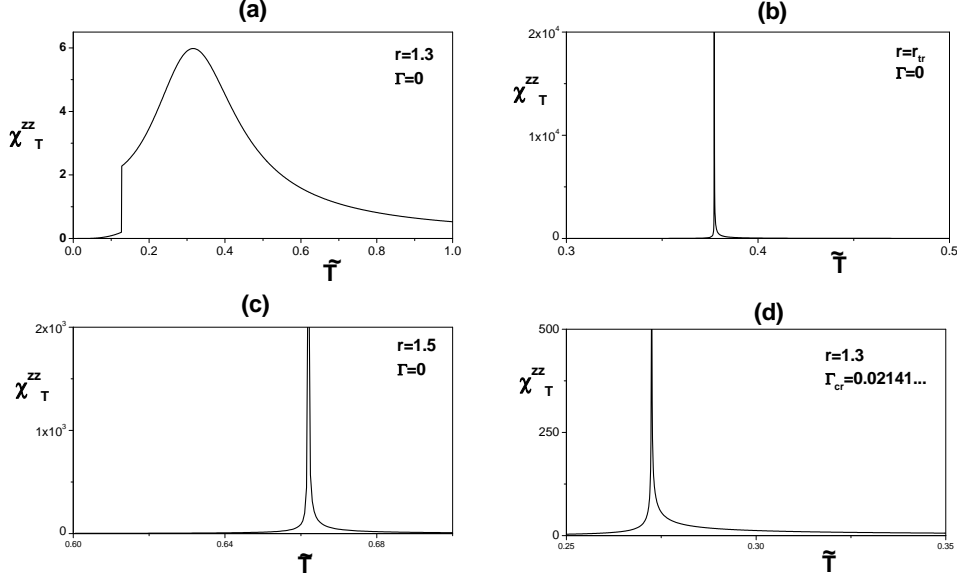


Figure 3: Isothermal susceptibility χ_T^{zz} , at zero field, as a function of temperature. (a) For $r=1.3$ ($r = I/J$) where the system undergoes a classical first-order transition. (b) At the tricritical point. (c) For $r=1.5$ where the system undergoes a classical second-order transition at zero field. (d) At the critical field Γ_{cr} ($\Gamma_{cr} = h_{cr}/J$, $\Gamma_{cr} = 0.02141\dots$) for $r=1.3$.

where

$$\varphi_t = \arccos[-(\Gamma_t + 2rM_t^z)]. \quad (37)$$

This first-order quantum line meets the classical first-order line in the plane $T = 0$, at $\Gamma = 0$ and $r = 4/\pi$. This result is easily verified by making $M_t^z = 0$ in eq.(36b). This line also meets the second-order line at $r = 0$ and $\Gamma = 1$. At this point it also meets the critical classical line, so that it is called a bicritical point since it corresponds to the intersection of two second-order critical lines. The phase diagram for these quantum transitions is shown in Fig.4 [16].

The magnetization as a function of the field is shown in Fig.5(a), where we can see the different types of critical behaviour. For $r < 0$, the magnetization is continuous, since we have second-order transitions, and it is discontinuous for $r > 0$, where we have first-order transitions. As in the classical behaviour, there are hysteresis cycles associated with these quantum first-order transitions, whose limits are obtained by determining the values of the fields at which the metastable states disappear. In order to analyze the critical behaviour of the system for $r < 0$, where it undergoes second-order quantum transitions, we define

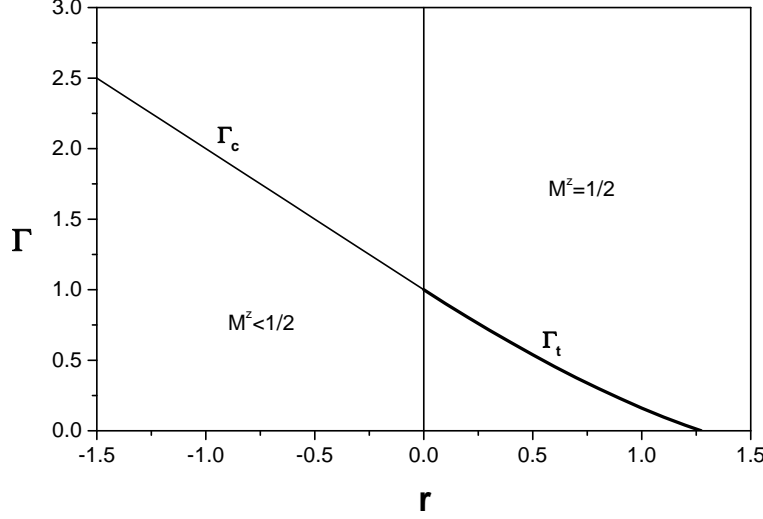


Figure 4: Phase diagram for the quantum transitions as a function of the strength of the long-range interaction r ($r = I/J$). Γ_t identifies the first-order transitions and Γ_c the second-order transitions.

the appropriate order parameter [17]

$$\widetilde{M^z} \equiv \frac{1}{2} - M^z, \quad (38)$$

which goes to zero ($\widetilde{M^z} \rightarrow 0^+$) as the field approaches to the critical field. Therefore, by expanding eq. (35) up to second-order in this parameter, we obtain

$$\frac{\pi^2}{2} \left(\widetilde{M^z} \right)^2 - 2r \widetilde{M^z} = \Gamma_c - \Gamma \geq 0, \quad (39)$$

where $\Gamma_c = 1 - r$. This result reduces to the known one for $r = 0$, namely, $\Gamma_c = 1$. The critical exponent β is easily obtained from the previous expression, and it is given by $\beta = 1/2$ for $r = 0$ and $\beta = 1$ for $r \neq 0$ [16]. In passing we would like to mention that if we treat the term $2IM^z$ as an external field h' , as pointed out by Suzuki [5], we can define an effective field $h_{eff} = h + h'$. In terms of this new field variable the magnetization becomes a universal curve, even when we have first-order transitions. The collapse of the magnetization curves, shown in Fig.5(a), is presented in Fig. 5(b) and could also be obtained directly from the equation of state. This rather important result clearly suggests that the quantum critical behaviour is associated with the effective field $h_{eff} = h + 2M^z I'$ ($\Gamma_{eff} \equiv h_{eff}/J = \Gamma + 2M^z r$), since along the critical line the magnetization is saturated.

In contrast to the behaviour in the classical transitions, the isothermal susceptibility,

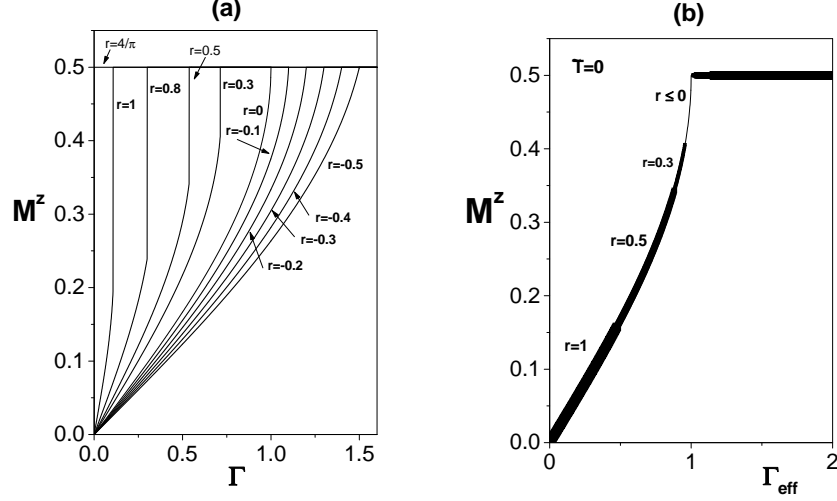


Figure 5: (a) Magnetization as a function of Γ ($\Gamma = h/J$), at $(\tilde{T} = k_B T/J)$ $\tilde{T} = 0$ and for different values of r ($r = I/J$), in the regions where the system undergoes first ($r > 0$) and second-order ($r \leq 0$) quantum transitions. (b) Universal curve for the magnetization as a function of the effective field Γ_{eff} ($\Gamma_{eff} = \Gamma + 2rM^z$) for $r > 0$ and $r \leq 0$.

obtained from eq. (34), and given by

$$\chi_T^{zz} = -\frac{\frac{1}{\pi} \frac{1}{\sqrt{1-(\Gamma+2rM^z)}}}{1 - \frac{2r}{\pi} \frac{1}{\sqrt{1-(\Gamma+2rM^z)}}}, \quad \text{or} \quad \Gamma < \Gamma_c, \quad (40)$$

diverges at the quantum second-order transition, for $r = 0$ only. This can be seen in Fig. 6, where the isothermal susceptibility, shown for different values of r , is finite for $r \neq 0$. This immediately implies that the critical exponent γ , defined as $\chi_T^{zz} \sim |\Gamma_c - \Gamma|^\gamma$, is equal to zero, for $r \neq 0$, and equal to $1/2$, for $r = 0$. Bearing in mind that, at $T = 0$, α is identical to γ , it can be shown that the exponents α, β and γ also satisfy the Rushbrook scaling relation [10]. It should be noted that the previous expression can also be obtained by taking $\tilde{T} \rightarrow 0$ in eq. (30). Finally, it is worth to mention that, by using eqs. (33), (34) and (36), we can determine the internal energy u at $T = 0$. Since it is equal to the Helmholtz free energy, $u = f$ is a continuous function of h independently of the order of the transition. However, at the first-order transition, its derivative (du/dh) is discontinuous. Explicitly, close to the critical field h_t , we can write

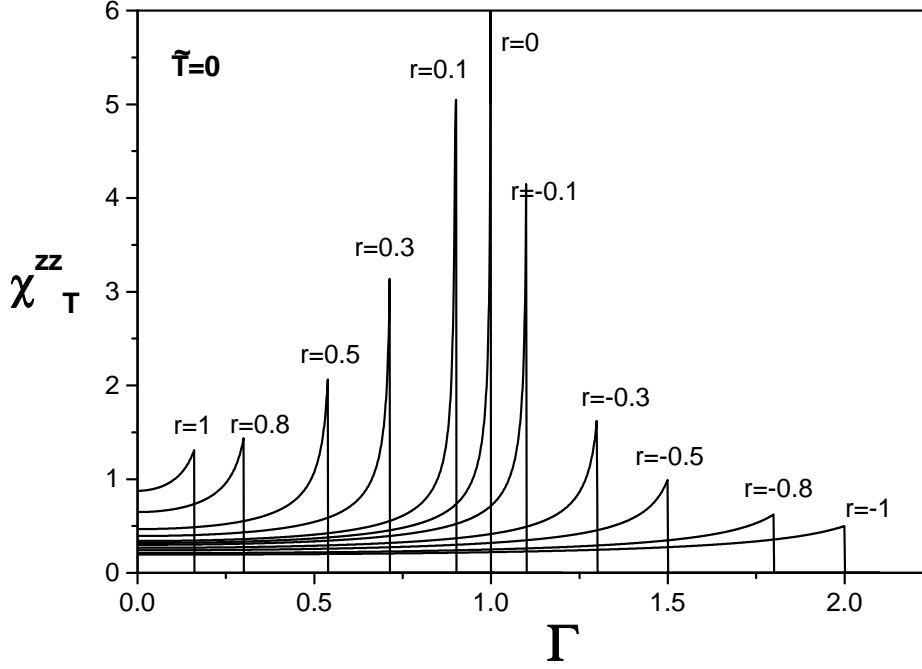


Figure 6: Isothermal susceptibility χ_T^{zz} , at $\tilde{T} = 0$ ($\tilde{T} = k_B T/J$), as a function of the field Γ ($\Gamma = h/J$) for different values of r ($r = I/J$).

$$f(h^-) \cong f(h_t) + M_t |h - h_t|, \quad \text{for } h < h_t, \quad (41a)$$

$$f(h^+) \cong f(h_t) - \frac{|h - h_t|}{2}, \quad \text{for } h > h_t, \quad (41b)$$

which satisfy the scaling relations recently proposed by Continentino and Ferreira [18] for first-order quantum transitions, with a critical exponent $\alpha=1$.

5 The dynamic correlation $\langle S_j^z(t) S_l^z(0) \rangle$

The dynamic correlation $\langle S_j^z(t) S_l^z(0) \rangle$ is defined as

$$\langle S_j^z(t) S_l^z(0) \rangle = \langle \exp(-iHt) S_j^z \exp(iHt) S_l^z \rangle, \quad (42)$$

where H is the Hamiltonian of the system. Since the long-range interaction term commutes with H , the dynamic correlation can be written as

$$\langle S_j^z(t) S_l^z(0) \rangle = \langle \exp(-iH't) S_j^z \exp(iH't) S_l^z \rangle, \quad (43)$$

where H' is given by

$$H' = -J \sum_{j=1}^N (S_j^x S_{j+1}^x + S_j^y S_{j+1}^y) - h \sum_{j=1}^N S_j^z S_{j+1}^z. \quad (44)$$

In terms of fermion operators, and introducing the Fourier transform, we can write H' in the form

$$H' = \sum_k \lambda_k c_k^\dagger c_k + \frac{Nh}{2}, \quad (45)$$

where

$$\lambda_k = -J \cos(k) - h. \quad (46)$$

From these results, it follows that

$$c_k(t) = \exp(-i\lambda_k t) c_k, \quad (47a)$$

$$c_k^\dagger(t) = \exp(i\lambda_k t) c_k^\dagger. \quad (47b)$$

Therefore, in terms of these operators, we have

$$S_j^z(t) = \frac{1}{N} \sum_{kk'} \exp[ij(k - k')] \exp(i\lambda_k t) \exp(-i\lambda_{k'} t) c_k^\dagger c_{k'} - \frac{1}{2}. \quad (48)$$

From this expression, the dynamic correlation is written as

$$\begin{aligned} \langle S_j^z(t) S_l^z(0) \rangle &= \frac{1}{N^2} \sum_{kk'qq'} \exp[ij(k - k')] \exp[i(\lambda_k - \lambda_{k'})t] \times \\ &\times \exp[il(q - q')] \langle c_k^\dagger c_{k'} c_q^\dagger c_{q'} \rangle - \frac{1}{N} \sum_{k'} \langle c_k^\dagger c_k \rangle + \frac{1}{4}. \end{aligned} \quad (49)$$

Introducing the Gaussian transformation and using Wick's theorem [13], the previous expression can be written in the final form

$$\begin{aligned} \langle S_j^z(t) S_l^z(0) \rangle &= \left[\frac{1}{N} \sum_k \langle n_k \rangle - \frac{1}{2} \right]^2 + \\ &+ \frac{1}{N^2} \sum_{kk'} \{ [\exp[ik(j - l)] \exp(i\lambda_k t) \langle n_k \rangle] \times, \\ &\times [\exp[-ik'(j - l)] \exp(-i\lambda_{k'} t) (1 - \langle n_{k'} \rangle)] \times \\ &\times \exp[-ik'(j - l)] \exp(-i\lambda_{k'} t) (1 - \langle n_{k'} \rangle)] \} \end{aligned} \quad (50)$$

where n_k is given by eq. (24b).

The static correlation $\langle S_j^z(0)S_l^z(0) \rangle$ is obtained from the previous expression. After some straightforward algebraic manipulations [19], can be written as

$$\begin{aligned} \langle S_j^z S_l^z \rangle = \frac{1}{4} \left\{ \left[\frac{1}{N} \sum_k \tanh \left(\frac{\bar{\epsilon}_k}{2} \right) \right]^2 - \right. \\ \left. - \left[\frac{1}{N} \sum_k \cos [k(j-l)] \tanh \left(\frac{\bar{\epsilon}_k}{2} \right) \right]^2 \right\}. \end{aligned} \quad (51)$$

For large separations, the correlation tends to the square of the magnetization. At $T = 0$, for $r + \Gamma < 1$ and $r < 0$, the direct correlation, $\rho^z(j-l) = \langle S_j^z S_l^z \rangle - \langle S_j^z \rangle^2$, can be expressed as

$$\begin{aligned} \rho^z(j-l) = - \left\{ \frac{\sin [(j-l) \arccos(\Gamma_{eff})]}{\pi(j-l)} \right\}^2 \\ = \frac{\exp [2i(j-l) \arccos(\Gamma_{eff})] + \exp [-2i(j-l) \arccos(\Gamma_{eff})] - 2}{4\pi^2(j-l)^2}. \end{aligned} \quad (52)$$

From this expression, and following Lima and Gonçalves [17], we can define an analytical extension for the scaling form of the direct correlation,

$$\rho(n) = \frac{F(in/\xi)}{n^p}, \quad (53)$$

where $p = d + z - 2 + \eta$. From this result and eq.(52), we obtain

$$(\xi)^{-1} = 2 \arccos(\Gamma), \quad (54)$$

which gives at the critical point, where $\xi \rightarrow \infty$, $\Gamma_{eff}^c = 1$ ($\Gamma_{eff} = \Gamma_c + r$). Using the scaling relation $\xi \sim |\Gamma_{eff} - \Gamma_{eff}^c|^{-\nu}$, we obtain $\nu = 1$ for $r \neq 0$, whereas $\nu=1/2$ for $r = 0$. The main implication of this result is that the dynamical exponent z , obtained from the exponent relation $\nu(z+d) = 2 - \alpha$ [20], is $z=1$ for $r \neq 0$ and $z=2$ for $r = 0$. Consequently, the system presents a non-universal critical dynamical behaviour. Also it should be noted that these spatial oscillations have been observed in the XXZ model with short-range interactions only [21].

The real and imaginary parts of $\langle S_j^z(t)S_l^z(0) \rangle$ can be explicitly written in the form

$$\begin{aligned}
Re\langle S_j^z(t)S_l^z(0) \rangle &= \left[\frac{1}{N} \sum_k \langle n_k \rangle - \frac{1}{2} \right]^2 + \left\{ \left[\frac{1}{N} \sum_k \cos[k(j-l)] \cos(\lambda_k t) \langle n_k \rangle \right] \times \right. \\
&\quad \times \left[\frac{1}{N} \sum_{k'} \cos[k'(j-l)] \cos(\lambda_{k'} t) (1 - \langle n_{k'} \rangle) \right] \Big\} + \\
&\quad + \left\{ \left[\frac{1}{N} \sum_k \cos[k(j-l)] \sin(\lambda_k t) \langle n_k \rangle \right] \times \right. \\
&\quad \times \left[\frac{1}{N} \sum_{k'} \cos[k'(j-l)] \sin(\lambda_{k'} t) (1 - \langle n_{k'} \rangle) \right] \Big\}, \tag{55}
\end{aligned}$$

and

$$\begin{aligned}
Im\langle S_j^z(t)S_l^z(0) \rangle &= \left[\frac{1}{N} \sum_k \cos[k(j-l)] \sin(\lambda_k t) \langle n_k \rangle \right] \times \\
&\quad \times \left[\frac{1}{N} \sum_{k'} \cos[k'(j-l)] \cos(\lambda_{k'} t) (1 - \langle n_{k'} \rangle) \right] + \\
&\quad - \left[\frac{1}{N} \sum_k \cos[k(j-l)] \cos(\lambda_k t) \langle n_k \rangle \right] \times \\
&\quad \times \left[\frac{1}{N} \sum_{k'} \cos[k'(j-l)] \sin(\lambda_{k'} t) (1 - \langle n_{k'} \rangle) \right]. \tag{56}
\end{aligned}$$

From these expressions we immediately conclude that, at $T = \infty$, the dynamic correlation is real and that, for arbitrary temperatures, $Im\langle S_j^z(t)S_l^z(0) \rangle \rightarrow 0$ and $Re\langle S_j^z(t)S_l^z(0) \rangle \rightarrow \langle S_j^z \rangle^2$ as $t \rightarrow \infty$. For classical second-order transitions and zero field, this result is shown in Fig.7 for the autocorrelation function, which is similar to the one at the tricritical point, along the critical line and when we have first-order classical transitions. It also should be noted that in the region where the system does not order the imaginary part goes to zero. The results for second-order quantum transitions are shown in Fig.8 and present essentially the same behaviour observed for the classical transitions irrespective of the order of the transition.

6 The longitudinal dynamic susceptibility

The dynamic susceptibility $\chi_q^{zz}(\omega)$ is obtained by considering the time Fourier transform of the two-spin correlation $\langle S_j^z(t)S_l^z(0) \rangle$, which is given by

$$\langle S_j^z S_l^z \rangle_\omega = \frac{1}{2\pi} \int_{-\infty}^{\infty} \langle S_j^z(t)S_l^z(0) \rangle \exp(i\omega t) dt. \tag{57}$$

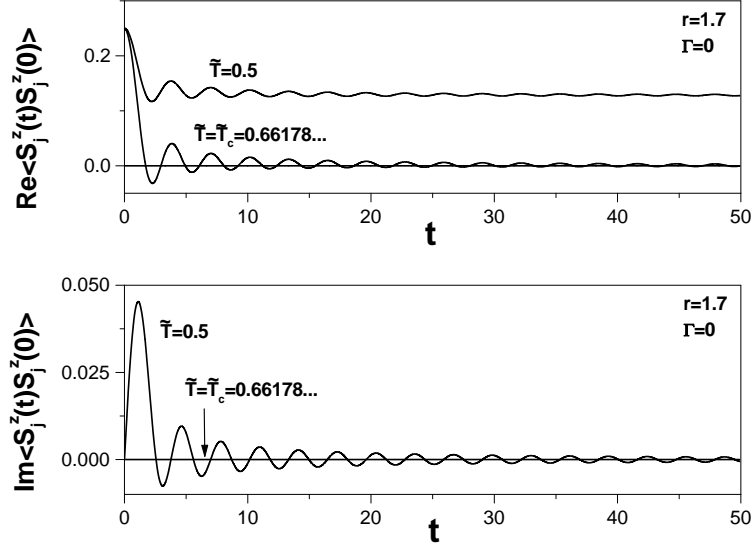


Figure 7: Real and imaginary parts of the autocorrelation function $\langle S_j^z(t)S_j^z(0) \rangle$ as a function of t , for $\Gamma = 0$, $r = 1.7$ ($\Gamma = h/J$, $r = I/J$), at the second-order transition temperature $\tilde{T}_c = 0.66178$. ($\tilde{T} = k_B T/J$) and at $\tilde{T} = 0.5$.

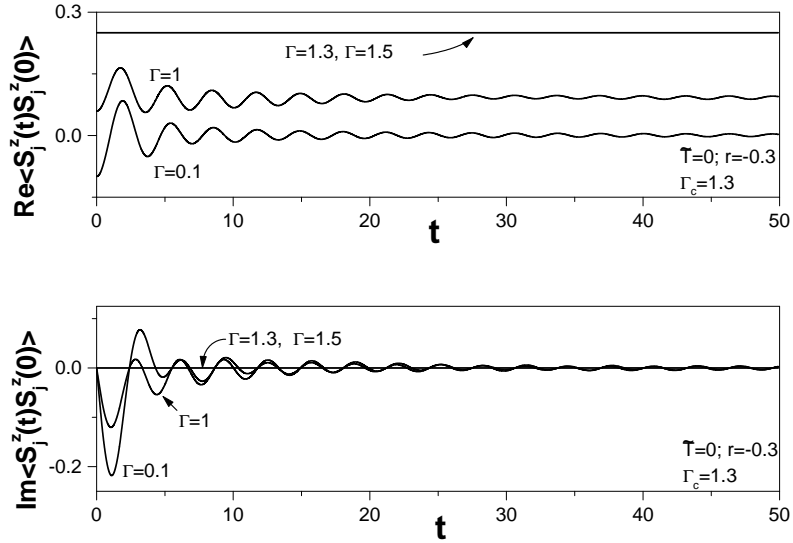


Figure 8: Real and imaginary parts of the autocorrelation function $\langle S_j^z(t)S_j^z(0) \rangle$ as a function of t , at $\tilde{T} = 0$ ($\tilde{T} = k_B T/J$) and $r = -0.3$ ($r = I/J$), for $\Gamma = 1.5; 1.0; 0.1$ ($\Gamma = h/J$), and at the second-order quantum transition ($\Gamma_c = 1.3$).

From this equation we obtain

$$\langle S_j^z S_l^z \rangle_\omega = \delta(\omega) \langle S_j^z \rangle^2 + \frac{1}{N^2} \sum_{kk'} \exp[i(k+k')(j-l)] \langle n_k \rangle (1 - \langle n_{k'} \rangle) \delta(\omega + \epsilon_k - \epsilon_{k'}). \quad (58)$$

Introducing the spatial Fourier transform,

$$\langle S_q^z S_{-q}^z \rangle_\omega = \frac{1}{N} \sum_{j-l} \exp[-iq(j-l)] \langle S_j^z S_l^z \rangle_\omega, \quad (59)$$

we obtain

$$\langle S_q^z S_{-q}^z \rangle_\omega = \delta(\omega) \langle S_{q=0}^z \rangle^2 + \frac{1}{N} \sum_k \delta(\omega + \epsilon_k - \epsilon_{k-q}) \langle n_k \rangle (1 - \langle n_{k-q} \rangle). \quad (60)$$

From this expression, we can write the susceptibility [22],

$$\begin{aligned} \chi_q^{zz}(\omega) &= -2\pi \ll S_q^z; S_{-q}^z \gg \\ &= -2\pi \frac{1}{2\pi} \int_{-\infty}^{\infty} \frac{[\exp(\beta\omega') - 1] \exp(-\beta\omega') \langle S_q^z S_{-q}^z \rangle_{\omega'}}{\omega - \omega'} d\omega', \end{aligned} \quad (61)$$

which leads to

$$\chi_q^{zz}(\omega) = -\frac{1}{N} \sum_k \frac{\langle n_k \rangle - \langle n_{k-q} \rangle}{\omega + \epsilon_k - \epsilon_{k-q}}. \quad (62)$$

The static susceptibility, $\chi_q^{zz}(0)$, is obtained from the previous expression by considering $\omega = 0$ and, in particular, $\chi_0^{zz}(0)$ is determined by taking the limit $q \rightarrow 0$, which gives, in the thermodynamic limit, the result

$$\chi_0^{zz}(0) = \frac{1}{4\pi\tilde{T}} \int_0^\pi \text{sech}^2 \left(\frac{\cos(k) + \Gamma + 2rM^z}{2\tilde{T}} \right) dk, \quad (63)$$

which is different from the isothermal susceptibility χ_T^{zz} shown in eq. (30).

Differently from the isothermal susceptibility, $\chi_q^{zz}(0)$ does not present any infinite singularity at the critical classical point. At the first-order classical transition, $\chi_q^{zz}(0)$ is discontinuous irrespective of the wave-vector, and presents a cuspid at the second-order classical transition ($\tilde{T} = \tilde{T}_c$).

At the quantum first-order transition points ($\Gamma = \Gamma_t$), $\chi_q^{zz}(0)$ is discontinuous, but finite, for any wave-vector. However, at the second-order quantum transitions ($\Gamma = \Gamma_c$), $\chi_q^{zz}(0)$ diverges at the critical point for $q = 0$ only.

The real and imaginary parts of $\chi_q^{zz}(\omega)$ are obtained from eq. (62) by considering $\chi_q^{zz}(\omega - i\epsilon)$ in the limit $\epsilon \rightarrow 0$. We have the explicit result

$$\text{Re}\chi_q^{zz}(\omega) = -\frac{1}{N} P \sum_k \frac{\langle n_k \rangle - \langle n_{k-q} \rangle}{\omega + \epsilon_k - \epsilon_{k-q}}, \quad (64)$$

where P denotes Cauchy principal value, and

$$Im\chi_q^{zz}(\omega) = \frac{\pi}{N} \sum_k (\langle n_k \rangle - n_{k-q}) \delta(\omega + \epsilon_k - \epsilon_{k-q}). \quad (65)$$

As in the isotropic model without long-range interactions on the alternating superlattice, $\chi_q^{zz}(\omega)$ goes to zero [23] for $\Gamma > \Gamma_c$ and for $\Gamma < \Gamma_c$, and $Im\chi_q^{zz}(\omega)$ is zero for $\omega > 2J \sin(q/2)$. No significant differences in the behaviour of the dynamic susceptibility are present in the classical and quantum regions. There are no infinite singularities in the imaginary part, and the finite discontinuities at the band edges correspond to finite (lower edge) and infinite (upper edge) divergences of the real part.

7 The classical-quantum crossover

The global phase diagram, in the space generated by temperature \tilde{T} , field Γ and ratio r between short and long-range interaction, is presented in Fig.9. The critical surface has a mirror symmetry with respect to the plane $\tilde{T} \times r$. As we can see, the classical second-order critical line meets the quantum critical line at P_{bc} . Therefore, P_{bc} is a bicritical point as previously conjectured [16]. As shown in Fig. 5(b), there is a universal curve for the magnetization, at $T = 0$, in terms of the effective field Γ_{eff} ($\Gamma_{eff} \equiv \Gamma + 2M^z r$). This gives support to the conclusion that Γ_{eff} is the relevant variable, as far as the critical behaviour is concerned. Therefore, the critical line can be drawn as a function of Γ_{eff} . It will end at the quantum critical point, $\Gamma_{eff} = 1$, for the second-order transitions. Similarly, the classical first-order transition line will end up at $\Gamma_{eff} = 4/\pi$, for $\Gamma = 0$, and the critical surface can be collapsed into two (two-dimensional) diagrams respectively related to the first and second-order transitions.

In these diagrams, which are characteristic of the quantum/classical phase transitions, there are different regions where either classical or quantum fluctuations dominate [24]. These regions are separated by crossover lines which, in general, are not so easily defined, since there is no unique criterion to characterize them [25]. In our case, we have defined a criterion from the behaviour of the magnetization as a function of temperature for different values of Γ , in different critical regimes.

For $r=-0.1$, where we have a second-order quantum transition, the magnetization as a function of the field for different values of Γ is shown in Fig. 10(a). The main feature is the appearance of a peak in the magnetization which disappears at the critical effective field $\Gamma_{eff} = 1$, which corresponds in this case to $\Gamma = 1.1$. For values of the field larger than this value, the magnetization is a decreasing monotonic function of temperature. In our view, this means that the classical behaviour has been set in from zero temperature. Therefore, we can associate the peaks in the magnetization with points of the crossover line which, in this case, separates the critical quantum and classical regimes. This critical classical/quantum diagram associated with the second-order transitions is shown in Fig.11(a). Since, at $\tilde{T} = 0$, the system is in an ordered quantum state for $\Gamma_{eff} < 1$, region I corresponds to the ordered quantum one where the quantum fluctuations predominate.

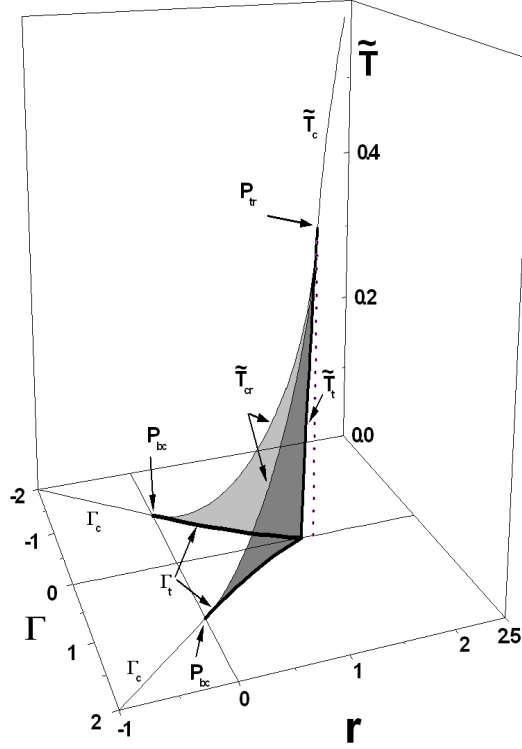


Figure 9: Global phase diagram of the model as a function of temperature \tilde{T} ($\tilde{T} = k_B T/J$), Γ ($\Gamma = h/J$) and r ($r = I/J$). \tilde{T}_t and \tilde{T}_c identify the first and second-order classical transitions, \tilde{T}_{cr} the classical critical line at nonzero field, P_{tr} the classical tricritical point. Γ_t and Γ_c identify the first and second-order quantum transitions and P_{bc} the quantum bicritical point.

Region II corresponds to the classical one where the classical fluctuations predominate. For $\tilde{T} = 0$ and $\Gamma_{eff} > 1$, the system is in the paramagnetic quantum state, but it becomes classical for $\tilde{T} \neq 0$. Consequently, this paramagnetic line coincides with the crossover line. For $r=1.0$, where we have a first-order quantum transition, the magnetization as a function of temperature presents a discontinuity in addition to the peak, as shown in in Fig. 10(b). As it can be seen in the inset of the Fig. 10(b), the peak of the magnetization will disappear for a field slightly smaller than the critical field Γ_c . This means that the crossover does not coincide with the second-order critical line shown in Fig. 11(a) as a function of Γ_{eff} , and ends at $\Gamma_{eff} = 1$. The first-order transition line ends at $\Gamma_{eff} = 4/\pi$, which is the quantum transition point; for $\Gamma_{eff} > 4/\pi$, the system is in the paramagnetic quantum state. The points along the axis $\tilde{T} = 0$, for $1 < \Gamma_{eff} < 4/\pi$, are first-order quantum transitions points; the classical/quantum critical diagram associated with the first-order transitions is shown in Fig. 11(b). As in Fig.11(a), region I corresponds to the ordered quantum state, where the quantum fluctuations predominate, and region II to the classical

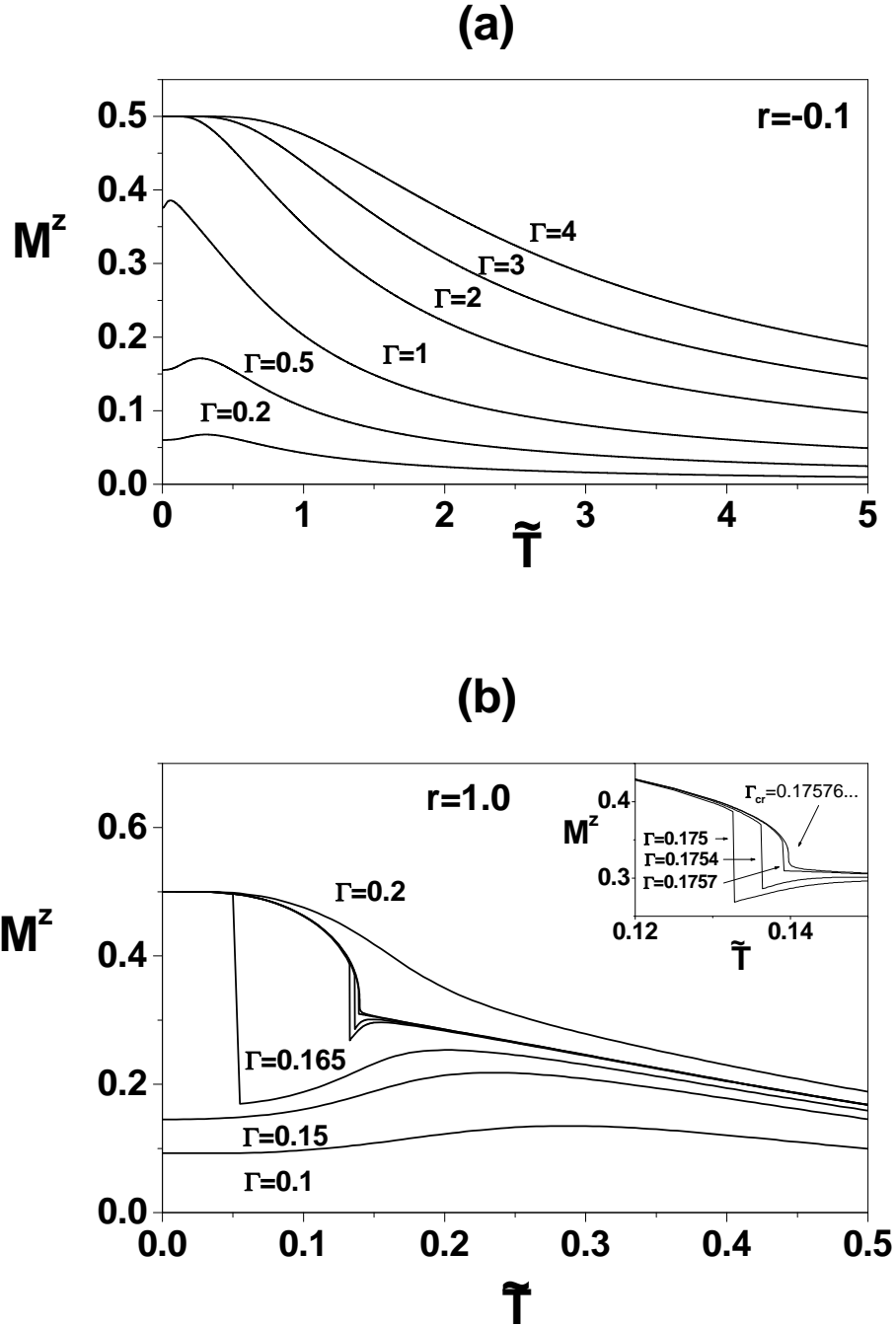


Figure 10: Magnetization as a function of temperature \tilde{T} ($\tilde{T} = k_B T/J$) for different values of the field. Γ ($\Gamma = h/J$). (a) For $r = -0.1$ ($r = I/J$) and (b) for $r = 1.0$.

one, where the classical fluctuations predominate. For $\Gamma_{eff} > 1$, as in the previous case, the crossover line coincides with the axis $\tilde{T} = 0$ since the system becomes classical for any $\tilde{T} \neq 0$.

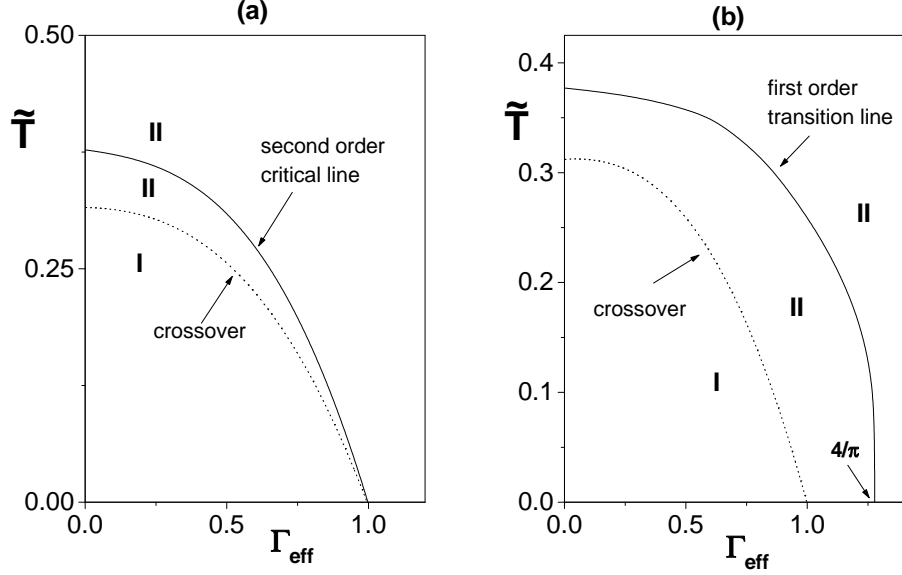


Figure 11: Phase diagrams for first and second-order transitions as function of Γ_{eff} ($\Gamma = h/J$, $r = I/J$, $\Gamma_{eff} = \Gamma + 2rM^z$). Region I corresponds to the quantum regime and region II to the classical regime. (a) Second-order transitions: for $\Gamma_{eff} > 1$, the crossover line coincides with the paramagnetic quantum line. (b) First-order transitions: for $\Gamma_{eff} > 1$, the crossover line coincides with the first-order quantum points ($1 < \Gamma_{eff} < 4/\pi$), and with the paramagnetic quantum line ($\Gamma_{eff} > 4/\pi$).

As we can see from Fig. 11, the phase diagrams for first and second-order classical/quantum transition present a similar structure. This new result gives support to the conjecture that there is a universal structure of the phase diagram associated with second-order quantum/classical transitions [1].

Acknowledgements

The authors would like to thank the Brazilian agencies CNPq, Capes and Finep for partial financial support. They would also like to thank Dr. A. P. Vieira for useful discussions and a critical reading of the manuscript.

References

- [1] S. Sachdev, Quantum Phase Transitions (Cambridge University Press, Cambridge, 1999).
- [2] See e.g. N. F. Mott, Metal-insulator Transitions, 2nd. ed. (Taylor & Francis, London, 1999).
- [3] A. P. Young, Lecture Notes on Quantum Phase Transitions, (International Centre for Theoretical Physics, Trieste, 1997).
- [4] S. L. Sondhi, S. M. Girvin, J. P. Carini and D. Sharkar, Rev. Mod. Phys. **69**, 315 (1997).
- [5] M. Suzuki, J. Phys. Soc. Jpn. **21**, 2140 (1966).
- [6] P. Jordan, E. Wigner, Z. Physik **47**, 631 (1928).
- [7] E. Lieb, T. Schultz, D. Mattis, Ann. Phys. **16** (1961) 407.
- [8] See e.g. D. J. Amit, Field Theory, the Renormalization Group, and Critical Phenomena (World Scientific, Singapore, 1984)
- [9] J. D. Murray, Asymptotic Analysis, Applied Mathematical Sciences, Vol.48 (Springer-Verlag, Berlin, 1984).
- [10] H. E. Stanley, Phase Transitions and Critical Phenomena (Oxford University Press, Oxford, 1971).
- [11] S. Katsura, T. Horiguchi and M. Suzuki, Physica **46**, 67 (1970).
- [12] J. F. Nagle, Phys. Rev. A **2**, 2124 (1970).
- [13] R. D. Mattuck, A Guide to Feynman Diagrams in the Many-body Problem, 2nd Edition (Dover Publications, New york, 1992).
- [14] L. L. Gonçalves and A. P. Vieira, J. Magn. & Magn. Mater. **177-181**, 76 (1998).
- [15] Th. Niemeijer, Physica **37**, 377 (1967).
- [16] L. L. Gonçalves, A. P. Vieira and L. P. S. Coutinho, J. Magn. Magn. Mater. **226-230**, 613 (2001).
- [17] J. P. de Lima and L. L. Gonçalves, Mod. Phys. Lett. B **8**, 871 (1994).
- [18] M. A. Continentino and A. S. Ferreira, cond-mat/0403272 (2004), to appear in Physica A.
- [19] L. P. S. Coutinho, MSc Thesis, Universidade Federal do Ceará (2001) in portuguese.

- [20] M. A. Continentino, Phys. Rep. **239**, 178 (1994).
- [21] K. Fabricius, A. Klümper and B. M. McCoy, Phys. Rev. Lett. **82**, 5365 (1999).
- [22] D. N. Zubarev, Sov. Phys. Usp. **3**, 320 (1960).
- [23] J. P. de Lima and L. L. Gonçalves, Physica A **311**, 458 (2002).
- [24] A. P. Young, J. Magn. & Magn. Mater. **226-230**, 556 (2001).
- [25] K. Fabricius and B. M. McCoy, Phys. Rev. B **59**, 381 (1999).